JCI insight

Mesenchymal stromal cell exosomes prevent and revert experimental pulmonary fibrosis through modulation of monocyte phenotypes

Nahal Mansouri, … , Alex Mitsialis, Stella Kourembanas

JCI Insight. 2019. https://doi.org/10.1172/jci.insight.128060.

Research In-Press Preview Pulmonology Stem cells

Mesenchymal stromal/stem cell (MSC) therapy has shown promise in experimental models of idiopathic pulmonary fibrosis (IPF). The aim of this study was to test the therapeutic effects of MSC-extracellular vesicles/exosomes (MEx) in a bleomycin-induced pulmonary fibrosis model and investigate putative mechanisms of action. Exosomes were isolated from media conditioned by human bone marrow MSCs. Adult mice (C57BL/6 strain) were challenged with endotracheal instillation of bleomycin and treated with MEx concurrently or for reversal models, at day 7 or 21. Experimental groups were assessed at day 7 and/or at day 14 or 28. Bleomycin-challenged mice presented with severe septal thickening and prominent fibrosis, and this was effectively prevented or reversed by a single dose of MEx. Furthermore, MEx therapy modulated whole lung macrophage phenotype and shifted the proportion of lung 'proinflammatory' classical monocytes, non-classical monocytes and alveolar macrophages to favor the monocyte/macrophage profiles of untreated-control mice. A parallel immunomodulatory effect was demonstrated in the bone marrow. Notably, transplantation of MEx-preconditioned bone marrow-derived monocytes alleviated core features of pulmonary fibrosis and lung inflammation. Proteomic analysis further revealed a signature enriched in non-inflammatory monocyte genes following MEx therapy supporting the immuno-regulatory, anti-inflammatory effect of MEx.We conclude that a bolus dose of MEx prevents and reverts core features of bleomycin-induced pulmonary fibrosis, and that the beneficial actions of MEx may be mediated via systemic […]

Mesenchymal Stromal Cell Exosomes Prevent and Revert Experimental Pulmonary Fibrosis Through Modulation of Monocyte Phenotypes

Nahal Mansouri[1,2,3,4,5], Gareth R. Willis[1,2], Angeles Fernandez-Gonzalez[1,2], Monica Reis [1,2], Sina Nassiri [4,6,] Alex Mitsialis[1,2] and Stella Kourembanas[1,2]

[1]*Division of Newborn Medicine & Department of Pediatrics, Boston Children's Hospital, Boston, USA.*

[2]*Department of Pediatrics, Harvard Medical School, Boston, USA.*

[3]*Pulmonary & Critical Care Medicine, Brigham & Women's Hospital, Boston, USA.*

[4] École polytechnique fédérale de Lausanne, Lausanne, Switzerland.

[5]Centre Hospitalier Universitaire Vaudois, Lausanne, Switzerland

[6]Bioinformatics Core Facility, SIB Swiss Institute of Bioinformatics, Lausanne, Switzerland.

Correspondence: Dr. Stella Kourembanas, Boston Children's Hospital, 300 Longwood Avenue, Division of Newborn Medicine, Boston, MA 02115. Tel: 617-919-2355. Fax: 617-730-0260. E-mail: Stella.Kourembanas@childrens.harvard.edu.

Conflict of Interest Statement: Drs. Mitsialis and Kourembanas are inventors of IP technology licensed by Boston Children's Hospital (BCH) to United Therapeutics Corp. As in all research studies, BCH has taken steps designed to ensure that any potential for financial gain does not undercut the validity and integrity of the information learned by this research.

Abstract

Mesenchymal stromal/stem cell (MSC) therapy has shown promise in experimental models of idiopathic pulmonary fibrosis (IPF). The aim of this study was to test the therapeutic effects of MSC-extracellular vesicles/exosomes (MEx) in a bleomycin-induced pulmonary fibrosis model and investigate putative mechanisms of action.

Exosomes were isolated from media conditioned by human bone marrow MSCs. Adult mice (C57BL/6 strain) were challenged with endotracheal instillation of bleomycin and treated with MEx concurrently or for reversal models, at day 7 or 21. Experimental groups were assessed at day 7 and/or at day 14 or 28.

Bleomycin-challenged mice presented with severe septal thickening and prominent fibrosis, and this was effectively prevented or reversed by a single dose of MEx. Furthermore, MEx therapy modulated whole lung macrophage phenotype and shifted the proportion of lung 'proinflammatory' classical monocytes, non-classical monocytes and alveolar macrophages to favor the monocyte/macrophage profiles of untreated-control mice. A parallel immunomodulatory effect was demonstrated in the bone marrow. Notably, transplantation of MEx-preconditioned bone marrow-derived monocytes alleviated core features of pulmonary fibrosis and lung inflammation. Proteomic analysis further revealed a signature enriched in non-inflammatory monocyte genes following MEx therapy supporting the immuno-regulatory, anti-inflammatory effect of MEx.

We conclude that a bolus dose of MEx prevents and reverts core features of bleomycin-induced pulmonary fibrosis, and that the beneficial actions of MEx may be mediated via systemic modulation of monocyte phenotypes.

Introduction

Idiopathic pulmonary fibrosis (IPF) is a chronic progressive respiratory disease that is characterized by clinical features such as shortness of breath, hypoxemia, radiographically evident pulmonary infiltrates, and continuing accumulation of fixed fibrosis (1-3). Arguably, the complex interplay between immune cell subsets, coupled with an incomplete understanding in disease pathophysiology have contributed to the paucity of successful therapies (4-6). In turn, IPF remains a fatal disease with, at present, a five-year survival rate of less than 10% from the time of diagnosis (7-9). Thus, with no effective therapy for either the prevention or treatment of IPF, the need for new therapies is paramount.

To this end, novel approaches are required to address this multifactorial progressive disease. Interestingly, in experimental models of pulmonary fibrosis, mesenchymal stromal/stem cell (MSC) therapy has shown promise, reducing lung collagen deposition, improving Ashcroft score, and decreasing inflammatory markers in bronchoalveolar lavage (10-14). Despite such physiological improvements in the recipient lung following MSC transplantation, there is a burgeoning awareness that the mechanism of therapeutic action is predominantly paracrine. Indeed, one of the major therapeutic modalities identified in the MSC secretome are extracellular vesicles (EVs), including exosomes, the EV subset that is generated through the endocytic/endosomal pathway (15-18). Recently, we and others have shown that intravenous (IV) delivery of purified human MSC-derived exosomes (MEx) has provided substantial functional and immunomodulatory benefits in several experimental models of lung disease (15,19-20) characterized by low levels of fibrosis. In this study, we utilize the murine bleomycin-induced lung injury model to investigate the therapeutic and immunomodulatory capacity of MEx on IPF pathology, a disease with prominent features of fibrosis.

Results

Purification, Isolation and characterization of exosomes

Exosomes were isolated from fraction 9 (F9) of concentrated cell culture supernatants after floatation on an iodixanol cushion (figure 1A). Transmission electron microscopy (TEM) and nanoparticle tracking analysis (NTA) revealed that both human bone marrow MSCs and human dermal fibroblasts (HDFs) gave rise to a heterogeneous exosome population that occupied a diameter of ~35–150 nm and exhibited the typical morphological features of exosomes (figure 1B, C). Purified MEx and fibroblast-derived exosome (FEx) fraction (F9) had comparable particle counts ($8.6 \pm 1 \times 10^{10}$ and $9.5 \pm 1 \times 10^{10}$ respectively) (figure 1A, data for FEx not shown). Immunoblots demonstrated that all exosome preparations were positive for established exosome markers (CD63, Alix, Flot1 and CD9) and lacked the cellular marker GM130 (figure 1D).

A bolus dose of MEx prevents and reverts bleomycin-induced pulmonary fibrosis

We used the murine bleomycin-induced experimental model of pulmonary fibrosis to assess the therapeutic capacity of MEx (21). First to evaluate the preventive effect of MEx, fourteen-week old mice received a single dose (endotracheal administration) of bleomycin (3 U/kg) or saline (vehicle control) on day 0. Mice that received bleomycin were compared to an untreated control group. Concurrent with bleomycin administration (day 0), treatment groups received a single IV dose of MEx, FEx, or exosome-free iodixanol vehicle. Mice were sacrificed at day 14 and lung sections were assessed for quantification of fibrosis (Masson's trichrome) and collagen content (schematic shown in figure 2A). Bleomycin-exposed mice demonstrated a histological pattern akin to human IPF, characterized by severe septal thickening and prominent fibrosis (figure 2B). Accordingly, compared to the control group, animals that received bleomycin presented with a greater Ashcroft score (1.76 ± 0.6 vs. 7.2 ± 0.3, $p < 0.001$, respectively, figure 2C) coupled with an elevated degree of collagen deposition (2.18 ± 0.09 vs. 3.02 ± 0.23 mg/ml, $p < 0.05$,

respectively, figure 2D). A single IV dose of MEx dramatically blunted the bleomycin-induced pulmonary fibrosis, improved the Ashcroft score (2.7 ± 0.6, $p< 0.0001$) and restored collagen content to levels similar to their untreated-counterparts (2.18 ± 0.15 mg/ml, $p< 0.05$). FEx and exosome-free iodixanol, served as biologic and treated-vehicle controls respectively, and had no effect on pulmonary fibrosis, Ashcroft score or collagen deposition ($p> 0.05$, figure 2B-D).

Given the critical role of apoptosis in the pathogenesis of fibrotic lung diseases (22,23) we also investigated the anti-apoptotic effect of MEx in the lung parenchyma. Here, both flow cytometric analysis of Annexin V and TUNEL staining in whole lung sections revealed that bleomycin-control mice presented with elevated levels of whole lung apoptosis compared to untreated control animals, and that MEx treatment efficiently reduced the degree of apoptosis (figure 2E-G).

In addition to the preventive capacity of MEx, we also assessed the ability of MEx to revert bleomycin-induced pulmonary fibrosis after the injury occurred. Here, following endotracheal bleomycin instillation at day 0, we administered a bolus dose of MEx at day 7 and assessed experimental groups at day 14 (schematic shown in figure 3A). Notably, a single MEx dose substantially reverted bleomycin-induced pulmonary fibrosis, improved the Ashcroft score ($p< 0.0001$) and restored collagen content to levels akin to their untreated-counterparts ($p< 0.05$, figure 3B-D).

We also sought to test the capacity of MEx to revert core features of bleomycin-induced pulmonary fibrosis at a ‘late rescue’ timepoint. Here, mice that received bleomycin (day 0) were given a bolus MEx dose at day 21 and assessed at day 28 (schematic shown in figure 3E). Compared to bleomycin control animals, ‘late rescue’ MEx treatment significantly reduced the bleomycin induced-elevation in collagen content ($p< 0.0001$, figure 3G), although no difference was noted in the Ashcroft score ($p> 0.05$, figure 3H).

MEx treatment modulates alveolar macrophage and monocyte populations in the lung

Alveolar macrophages (alveolar MΦ) and infiltrating monocytes play a pivotal role in pulmonary inflammation and in the development and progression of fibrosis (24-26). To investigate changes in immune cell populations following bleomycin-induced lung injury we performed whole lung cytometric analysis at days 7 and 14 in animals that received MEx at day 0. On day 7, compared to control mice, we noted a decrease in the proportion of alveolar MΦ and non-classical monocytes (defined as, $CD45^+$ $CD11b^-$ $CD11c^+$ $CD64^+$ cells and, $CD45^+$ $CD11b^+$ MHC II^- $CD64^{low/int}$ CCR-2^- $Ly6c^{low}$ cells, respectively) coupled with a concomitant increase in the number of 'proinflammatory' classical monocytes (defined as, $CD45^+$ $CD11b^+$ MHC II^- $CD64^{low/int}$ CCR-2^+ $Ly6c^{hi}$ cells) in bleomycin-exposed animals. MEx therapy effectively rescued all cell populations, increasing the levels of alveolar MΦ ($p< 0.01$) and non-classical monocytes ($p< 0.05$), whilst decreasing the number of classical monocytes comparable to controls ($p< 0.001$, figure 4A). Paradoxically, at day 14 (figure 4B), we found that the proportion of alveolar MΦ was increased ($p<0.05$) whilst the number of classical monocytes were reduced in bleomycin treated animals, compared to controls. Again, MEx therapy shifted the alveolar MΦ and monocyte profiles towards that of their untreated counterparts. Importantly, cytometric analysis showed that the overall percentage of $CD45^+$ monocytes did not change across the three experimental groups at either time-point (day 7 and day 14).

Administration of MEx modulates whole lung inflammation

To investigate the effect of MEx on pulmonary inflammation, whole lung mRNA levels were assessed at day 7 and day 14. We noted that gene expression levels of proinflammatory cytokines that were typically associated with activation of macrophages, such as *Ccl2* and arginase 1 (*Arg1*), were dramatically elevated in mice that received bleomycin compared to control animals at both day 7 or 14, and that this bleomycin-induced elevation was reduced by MEx administration ($p< 0.05$, figure 5 A, B). Interleukin 6 (*Il6*), showed a similar trend but the difference did not reach

statistical-significance between groups ($p > 0.05$). Transforming growth factor-ß (*Tgfb*) expression was similar at day 7 and day 14 between all experimental groups ($p > 0.05$, figure 5A, B). In accordance, immunofluorescence analysis of lung tissue sections showed a marked increase in the expression of CD206 and ARG1 proteins in bleomycin-exposed mice, which was effectively reduced by MEx therapy to levels akin to the control group ($p < 0.01$, figure 5C, D). As expected, bronchoalveolar lavage (BAL) protein content was increased in bleomycin-exposed mice as opposed to control. MEx therapy decreased the BAL total protein content ($p < 0.05$, figure 5E).

MEx therapy modulates monocyte population in the bone marrow

Recruited monocytes from the bone marrow to the lung have been associated with the pathophysiology of pulmonary fibrosis (24-27) and considering our finding that MEx therapy was associated with modulation of monocyte populations in the lung, we next investigated if intravenously-delivered MEx exert immunomodulatory actions directly on bone marrow progenitors. Here, mice were sacrificed at day 7 and myeloid cells in the bone marrow were assessed by flow cytometry.

Interestingly, bleomycin-exposed mice presented with dramatically reduced levels of non-classical monocytes present in the bone marrow compared to control animals (14.18 % ± 2.7 vs 32.3 % ± 5.5, $p<0.05$, respectively). A single dose of MEx therapy administered concomitantly with bleomycin, shifted the bone marrow non-classical monocyte profile (27.57 % ± 5.7, $p < 0.05$) towards that of their untreated counterparts. Moreover, the classical monocyte population in the bleomycin-exposed group was greater (67.8 % ± 1.7) than the control group (50.1 % ± 3.2, $p < 0.001$), and effectively suppressed by MEx therapy (57.5 % ± 3.9, $p < 0.05$, figure 6A). Notably, cytometric analysis showed that the proportion of total monocytes did not change across the three experimental groups (figure 6).

MEx therapy reprograms monocytes to a non-classical phenotype

Since MEx therapy was associated with a 'pro-homeostatic' shift in lung macrophage/monocyte phenotype and a concomitant rescued bone marrow non-classical monocyte population, we sought to determine whether MEx therapy affords such robust physiological changes in the lung by directly modulating the bone marrow-myeloid/monocyte (My/Mo) cell lineage phenotype. To investigate the modulatory effect of MEx on My/Mo populations, we preconditioned these cells with MEx ex vivo. Here, primary myeloid cells were isolated from the bone marrow of wild type (healthy) FVB mice aged 6-8 weeks. At day 0 of in vitro culture, the population of myeloid cells was heterogeneous with monocyte lineage accounting for approximately 24% of the cells in culture (BMDMy, data not shown). Cells were subsequently cultured for three days in the presence of macrophage colony stimulating factor (M-CSF) to drive the monocyte/MΦ lineage (28). Myeloid cells were treated with MEx or cell culture (MEx-free) medium alone (schematic shown in figure 7A) and confirmed to be $CD45^{+}$ and $CD11b^{+}$ by flow cytometry (>90% figure 7B). There was no difference in the number of viable cells and the degree of apoptosis between MEx treated or media (control) treated myeloid cells (data not shown). To understand the impact of MEx on My/Mo cells, we next profiled this cell lineage by performing proteome analysis after MEx treatment using Liquid Chromatography Tandem Mass Spectrometry (LC-MS/MS). To this end, we treated the My/Mo cells on day 1 and 2 with MEx (Figure 7A) or FEx (control) and harvested cells at day 3 for protein extraction. Analysis of the proteomic data revealed a signature composed of 84 features whose abundance varied significantly between MEx-treated My/Mo cells and FEx-treated controls (FDR<0.25, figure 7C). Interestingly, MEx-treatment was associated with lower abundance of multiple pro-inflammatory proteins such as those belonging to the mitogen-activated protein kinase (MAPK) and the serpin family. On the other hand, MEx increased the abundance of pro-regulatory proteins such as Mrc1 and CerS2. We next set out to test if this proteomic signature was indicative of either a classical or a non-classical phenotype in MEx-treated monocytes using publicly available transcriptome data of $Ly6c^{pos}$ and $Ly6c^{neg}$ bone marrow-derived monocytes (29). Indeed, gene set testing revealed that genes

encoding for the proteins overrepresented in the MEx-treated group were overexpressed in non-classical Ly6c^{neg} monocytes ($p<0.001$), whereas genes encoding for the proteins under-represented in MEx-treated My/Mo cells were overexpressed in classical Ly6c^{pos} monocytes ($p<0.001$) (figure 7D, S2). These results provide compelling evidence that the protective effects induced by MEx treatment are, at least in part, mediated by reprogramming of bone marrow-derived monocytes (BMDMo) to a non-classical phenotype.

Transplantation of bone-marrow derived-monocytes preconditioned with MEx prevents bleomycin-induced pulmonary fibrosis

Since our proteomic data indicated a primary effect of MEx on monocyte phenotypes within the bone-marrow derived myeloid populations, we sought to address whether the pro-modulatory effect of MEx on BMDMo is responsible for the prevention of fibrosis. We performed adoptive transfer experiments of BMDMo that were preconditioned with MEx (as shown in the schematic of figure 8A) *ex vivo* and delivered into the bleomycin-induced pulmonary fibrosis model. Mice that received 2 doses of BMDMo on days 0 and 3 after bleomycin injection were sacrificed at day 14 and lungs were assessed for histology and collagen content (figure 8). Compared to bleomycin-control mice, the group that received BMDMo preconditioned with MEx (BMDMo+MEx) presented with a drastically improved Ashcroft score (7.2 ± 0.3 vs. 3.5 ± 1, $p < 0.0001$, respectively) coupled with lower total collagen levels (3.02 ± 0.23 vs. 0.68 ± 0.41 mg/ml, $p < 0.001$, respectively). Interestingly, mice that received BMDMo-control (not preconditioned with MEx, (BMDMo+Media)), presented with evidence of partially reduced fibrosis, as assessed by the Ashcroft score ($p < 0.05$), however collagen deposition was similar between the two experimental groups (figure 8D,E).

To explore if the anti-fibrotic effect of MEx is due to resident alveolar MΦ, we also administered alveolar MΦ preconditioned with MEx (alveolar MΦ+MEx) endotracheally following bleomycin instillation. Again, alveolar MΦ were sourced from bronchoalveolar lavage fluid obtained from wild

type (healthy) FVB mice aged 6-8 weeks. Importantly, we did not detect any amelioration of fibrosis in mice who received preconditioned alveolar MΦ compared to the bleomycin group (figure 8C,D,E). To further assess the inflammatory changes in the lung after the administration of MEx-preconditioned BMDMo, we quantified the Cd68 and Retnla-expressing macrophages in the pulmonary parenchyma using immunofluorescent staining. Mice that received monocytes that were preconditioned with MEx showed reduced pulmonary macrophage numbers compared to BMDMo+Media-treated littermates ($p<0.05$, figure 9).

Discussion

Here, we demonstrate that a single IV dose of purified exosomes derived from human bone marrow MSCs, effectively prevented and reverted core features of bleomycin-induced pulmonary fibrosis, improving pulmonary morphology, blunting collagen deposition and restoring lung architecture. Furthermore, we show that MEx treatment is associated with an analogous modulation of lung and bone marrow monocyte populations. We demonstrated a shift in the proportion of infiltrating classical monocytes, non-classical monocytes and alveolar macrophages to favor the monocyte/macrophage profiles of untreated-control mice. We further extended our observations to show that the systemic modulatory role and 'pro-homeostatic' non-classical effect of MEx is primarily executed by the modulation of myeloid cell phenotype. Proteomic analysis of MEx-preconditioned monocyte revealed a signature indicative of pro-regulatory ($Ly6c^{low}$, non-classical) monocytes. Strikingly, we found that transplantation of BMDMo that were preconditioned by MEx prevented collagen deposition, restored lung architecture in bleomycin-exposed animals, and decreased inflammation.

Previous reports established that MSC/stem cell-based therapies has been effective in preventing experimental models of pulmonary fibrosis (11,13). Although the findings from this report should be judged in the context of the bleomycin experimental model used, our findings here are in accordance with our previous reports, which demonstrate that the MSC secretome harnesses the

prominent therapeutic modalities, and that the major therapeutic vector within the conditioned media is represented by the exosomes (15,18). The potent immunomodulatory role of MEx and MSC-conditioned media has been well recognized in preclinical models of bronchopulmonary dysplasia, pulmonary hypertension, cardiotoxin-induced skeletal muscle injury, and acute lung injury (19,30,31). In agreement, our present study not only suggests that MEx therapy modulates whole lung inflammation but demonstrates a novel immunomodulatory effect of MEx on lung and bone marrow monocyte populations. Specifically, we report that MEx therapy initiates an increase in non-classical monocytes and a concurrent reduction in proinflammatory monocytes in the bone marrow. This is associated with similar immunomodulatory effects in the lung and with drastic improvements in lung architecture and the subsequent prevention of bleomycin-induced pulmonary fibrosis. Interestingly, MEx-preconditioned monocytes exhibit a proteomic signature compatible with non-classical monocytes.

In experimental models of fibrosis, it is well recognized that recruitment of inflammatory ($Ly6C^{hi}$) monocytes and chronic activation of pro-remodeling macrophages play an important role in the development and progression of fibrosis (24-26,30,32-36). For example, using a diphtheria toxin receptor induced-acute kidney injury model, Lin and colleagues have shown that bone marrow $Ly6C^{hi}$ monocytes are selectively recruited to injured kidney and play a pivotal role in regulating fibrosis (36). Previous reports have also demonstrated that patients with IPF present with differential expression of monocyte/macrophage-specific markers (37), and that altered monocytic profiles may contribute to the pathogenesis of interstitial lung diseases (ILD) (38). More recent studies, investigating the transcriptome profile of monocyte/macrophage populations in a bleomycin model of pulmonary fibrosis, suggest that selectively targeting monocyte derived-alveolar MΦ differentiation may ameliorate pulmonary fibrosis (39).

The striking prevention of bleomycin-induced pulmonary fibrosis from transplantation of MEx-preconditioned BMDMo, implies that the systemic modulation of BMDMo phenotype is likely associated with the anti-fibrotic actions of MEx in the lung. Notably, no beneficial effects were

found with transplantation of MEx-preconditioned alveolar MΦ. In contrast, using a lipopolysaccharide-induced acute lung injury model, Morrison and colleagues recently demonstrated that endotracheal administration of alveolar MΦ preconditioned with MSC-EVs, decreased whole lung inflammation and bronchoalveolar lavage fluid protein (30). It is fair to speculate that this may be due to the differences in experimental models and subsequent underlying pathophysiology due to distinct MΦ phenotypes and mechanism of injury. Van de Laar *et al.,* demonstrated that both mature alveolar MΦ and BMDMo have the capacity to colonize an empty alveolar MΦ niche and develop into functional tissue-resident macrophages (40). Indeed, it is possible that the absence of an empty alveolar MΦ specific niche at the beginning of inflammation (day 0 to 3) in our model did not allow sufficient colonization by the transplanted alveolar MΦ. Furthermore, given our findings that 'normal' bone marrow contains a fraction (~32%) of non-classical monocytes, it is expected that the adoptive transfer of these monocytes, that have not been exposed to MEx, may confer some benefit. Although, this beneficial effect is much reduced when compared to MEx-preconditioned BMDMo. In agreement, we show that MEx therapy not only ameliorates total lung dysregulation of macrophage phenotype, it is associated with an analogous immunomodulatory effect on both the lung and bone marrow myeloid cell populations.

Bioinformatics analysis identified 84 proteins to be differentially abundant in MEx- versus FEx-preconditioned monocytes. This protein signature highlighted a decrease in pro-inflammatory state and an increase in pro-regulatory state of monocytes in response to MEx treatment. We could further establish an association between the MEx-induced proteomic signature and $Ly6C^{neg}$ pro-regulatory monocytes at the transcriptome level. Collectively, these analyses reinforce the hypothesis that MEx act directly on regulatory pathways to reprogram monocytes into an anti-inflammatory state. Further, findings from this report show that MEx, at least in part, via modulation of bone marrow and lung monocyte/macrophage profiles, suppress whole lung

inflammation to favor ‘pro-homeostatic’ myeloid population phenotypes, that is associated with the prevention and reversal of bleomycin-induced pulmonary fibrosis.

Deciphering the molecular mechanism of action and identifying any specific bioactive modalities responsible for the beneficial effects of MEx remains pending. We strongly believe that this beneficial effect is not exerted via one, but the constellation of mediators such as proteins and non-coding RNAs packaged in exosomes (41).

We noted the most remarkable results with early administration of MEx (day 0 and 7). Despite no improvement in Ashcroft score, we noted a significant reduction of collagen deposition with late administration of MEx (day 21). In the absence of inflammation in established fibrotic stage, we believe that other mechanisms such as nucleic acid transfer (41), inhibition of alveolar epithelial cell apoptosis (42), or promotion of endogenous growth factor secretion (43) may take part in the antifibrotic effect of MEx.

Future studies beyond the scope of this manuscript, should investigate how MEx may alter the epigenetic landscape and ‘regulatory’ gene expression of BMDMo. Additionally, the effect of MEx on other cell types in IPF such as lung epithelial cells and endothelial cells needs further investigation.

On balance, the application of exosomes represents an exciting and innovative approach to treat fibrotic lung diseases, especially considering that exosome-based therapeutics may obviate safety concerns associated with live cell treatments. However, we acknowledge a number of limitations in our study. Firstly, MEx dose was based on previous work using MEx in experimental models of bronchopulmonary dysplasia and pulmonary hypertension. However, for considering the clinical application of MEx, dose response experiments should be performed in future studies. Additionally, future experiments beyond the scope of this study, could investigate different routes of administration, specifically comparing endotracheal administration versus intravenous, to decipher if localized delivery is sufficient to afford systemic immunomodulatory benefits and ameliorate bleomycin-induced pulmonary fibrosis. It is worth mentioning that although our

isolation method mostly allows for the purification of extracellular vesicle in the exosomal range, due to overlap of exosomes with microvesicles in size and morphology, the presence of microvesicles in our preparation is very likely.

Our group and others have shown that MSC-exosomes distribute primarily to the lung, liver, and spleen [44,45]. It is plausible that MEx exert their upstream immunomodulatory effect in the bone marrow by reprogramming the myeloid cells to a pro-regulatory phenotype leading to lower lung infiltration of proinflammatory/profibrotic monocytes. An effective tool to track MEx in vivo, and accurately assess the bio-distribution remains elusive, and is an important question to address for potential monocyte/macrophage–targeted therapies.

On balance, findings described in this report provide new insights into the systemic immunomodulatory responses following bleomycin-induced lung injury and the subsequent non-classical effects of MEx-modulated monocyte phenotypes. Collectively, MEx treatment represents a promising cell-free therapy for the treatment of fibrotic lung diseases.

Methods

Exosome isolation and purification

Exosome isolation, purification and characterization were performed as previously described using iodixanol (OptiPrep™) cushion density floatation (19). Briefly, concentrated conditioned media from human bone marrow MSCs or HDFs were floated on an iodixanol cushion and centrifuged for 3.5 hours at 100,000 $\times$ *g* at 4°C. The exosome-containing fraction (Fraction 9, F9) was used for subsequent in vitro and in vivo experiments after confirming the presence of established exosome markers (Alix, CD63, CD9 and Flotillin-1 (FLOT1)) [(19)].

Bleomycin-induced pulmonary fibrosis model

Fourteen-week-old mice (C57BL/6 strain, Charles River Laboratories, MA) were anaesthetized with isoflurane and received a single endotracheal dose of bleomycin sulphate (50 µl, 3 U/kg) at day 0. Bleomycin naïve mice (control) received an endotracheal dose of saline (50 µl). Treated animals received a single IV (tail vein) dose of MEx, (200 µl, dose: 5×10^6 MSC equivalents, ~8.6×10^8 particles) at day 0. Human dermal fibroblast (HDF)-derived exosomes (FEx); (200 µl, dose: 5×10^6 HDF equivalents, ~9.2 x 10^8 particles) or exosome-free iodixanol vehicle only (200 µl, 10% w/v, IDX) served as biological and vehicle controls, respectively. Mice were assessed at day 7 and/or at day 14 or day 28 for cytometric, histological and/or RT-qPCR analysis.

Cell isolation and culture

Human bone marrow mesenchymal stem cells were obtained from RoosterBio (RoosterBio, MD, US). HDFs were established by tissue explant method (46). BMSCs and HDFs were cultured and expanded and further characterized as described previously (19).

Transmission electron microscopy (TEM)

An aliquot of 5-10 µl of the exosome preparation was adsorbed for 15 seconds on a formvar/carbon coated grid (Electron Microscopy Sciences, PA, US). Samples were stained with 2% uranyl acetate after removal of excess liquid with Whatman Grade 1 filter paper (Sigma). EVs were then viewed by a JEOL 1200EX transmission electron microscope (TEM), and images were recorded with an AMT 2k CCD camera.

Nanoparticle tracking analysis

Size and concentration distributions of exosomes were determined using nanoparticle tracking analysis (NTA, NanoSight LM10 system, Malvern instruments, MA, US) as described previously [19].

Western blot analysis

Proteins in exosome preparations were separated on a 4-20% polyacrylamide gel (Bio-Rad, Hercules, CA), followed by transfer to 0.45 µm PVDF membrane (Millipore, MA, US). Rabbit polyclonal anti-flotillin- 1 and anti-CD63 antibodies (Santa Cruz Biotech, CA, US, #25506 and #15363 respectively), and, mouse monoclonal anti-Alix, anti-CD9 and anti-GM130 antibodies (Santa Cruz Biotech, CA, US, #53538, #13118 and # 55590 resepectively) were used based on recommended dilutions by the manufacturer.

Exosome dosing

Exosome preparations were diluted on PBS to correspond to 5 x 10^6 cell equivalent. This dose was estimated based on our previous dose calculation in newborn mice with corresponding NTA and protein concentrations (19).

Histology

Mice were euthanized with intraperitoneal injection of pentobarbital at designated time points following the instillation of bleomycin. The hearts were perfused with phosphate-buffered saline (PBS, Invitrogen) through the right ventricle. Bronchoalveolar lavage (BAL) fluid was collected after the instillation of 3 ml of intratracheal PBS (5 gentle collection of 0.6ml), cells were discarded after ultracentrifugation and supernatant was stored for further analysis. BAL protein was quantified using pierce™ BCA protein assay (Thermo Fisher Scientific, Inc., Waltham, MA). For histologic analysis, the trachea was cannulated, and lungs were inflated with 4% paraformaldehyde (PFA) at a constant pressure with a tubbing connected to a PFA reservoir 25cm above the level of the mouse. The trachea was secured with a knot to avoid the drainage of PFA. The right lung was embedded in paraffin and sectioned for hematoxylin and eosin or Masson's trichrome staining. The left lung was either snap frozen in liquid nitrogen and used for RNA and protein isolation or used fresh for collagen quantification or cytometric analysis. Randomly selected areas (10-15 fields) from 5 μm thick lung sections were acquired at x100 and x200 magnification using a Nikon Eclipse 80i microscope (Nikon, Tokyo, Japan). For histologic quantification, the Ashcroft score was used in a blinded fashion. Scores of 0-1 represented no fibrosis, scores of 2-3 represented minimal fibrosis, scores of 4-5 were considered as moderate fibrosis, and scores of 6-8 indicated severe fibrosis.

Immunofluorescence staining

Lung tissue sections were de-paraffinized in xylene and rehydrated. Tissue slides were treated with 10 mM citrate buffer and blocked with serum and BSA for 20 minutes. Samples were then incubated at 4°C overnight with indicated primary antibody, Arginase 1 (Santa Cruz Biotech, CA, US, #20150); CD206 (Santa Cruz Biotech, CA, US, #58987), CD68 (Bio-Rad, CA, US, # MCA1957GA) and Retnla (Abcam, MA, US, #39626), then further incubated with secondary antibody (Life technologies, MA, US) for 20 minutes followed by nuclear staining with DAPI for 10 minutes. Arginase 1 (Arg-1) and CD206 positive cells were imaged using a Nikon Eclipse 80i

microscope (Nikon, Tokyo, Japan). Ten random images were analyzed using image J software. Mean Fluorescence Intensity (MFI) was calculated using the following formula: MFI = Integrated Density - (Area of selected cell x Mean fluorescence of background reading).

Sircol collagen assay

The left lung was used for collagen quantification per manufacturer's protocol (Bicolor, Life Science Assays). Briefly, left lung homogenate was shaken overnight at 4°C in 5 ml of 0.5 M acetic acid with 0.6% v/v pepsin. One ml of dye reagent was added to 100 µl of transparent supernatant and the samples were vortexed for 30 minutes. The residual pellet was washed by acid-salt wash buffer to eliminate unbound collagen and pH was normalized with alkalization buffer. Absorbance was measured at a wavelength of 550 nm in a microplate reader. Measured collagen content was compared to a standard curve and represented as mg/ml of left lung homogenate.

Cytometric analysis of mouse whole lung and bone marrow

Lung macrophage populations were assessed by flow cytometry as previously described [47]. Lungs were harvested on days 7 and 14. Left lung was cut into small pieces and digested in 5 ml of digestion buffer consisting of RPMI-1640 (Invitrogen, CA, US), Collagenase IV (1.6 mg/ml); and DNAse1 (50 unit/ml), (both from Worthington Biochemical Corp, NJ, US). Lung were shaken at 37°C for 30 min and red blood cells (RBC) were lysed using RBC lysis buffer (Roche, IN, US). Homogenized lung was passed through a 40 µm cell strainer (Corning, MA, US) to obtain a single-cell suspension.

For the assessment of Alveolar MΦ and monocyte populations, the cell suspension was stained with antibodies; PE/Cy7-conjugated anti-mouse CD45 (Biolegend, CA, US, #103114), FITC-conjugated anti-mouse CD11b (BD Biosciences, #553310), PerCP Cy 5.5-conjugated anti-mouse CD11c (BD pharmingen, #560584), BV 605-conjugated anti-mouse MHC II (Biolegend, #107639),

PE-conjugated anti-mouse CD64 (Biolegend, #139303), BV 421-conjugated anti-mouse CD24 (Biolegend, #101825), BV 510-conjugated anti-mouse Ly6C (Biolegend, #127627) and Alexa 647-conjugated anti-mouse CCR-2 (Biolegend, #150603).

For the evaluation of bone marrow derived monocytes (BMDMo), freshly flushed cells from the femur and tibia of adult mice were stained with PE/Cy7-conjugated anti-mouse CD45, FITC-conjugated anti-mouse CD11b, BV 605-conjugated anti-mouse MHC II, PE-conjugated anti-mouse CD64, BV 421-conjugated anti-mouse CD24, BV 510-conjugated anti-mouse Ly6C and Alexa 647-conjugated anti-mouse CCR-2.

Compensation was adjusted accordingly and supported by UltraComp ebeads (Affymetrix, CA, US). Fluorescence-minus-one controls were used accordingly. Cell populations were identified according to the gating strategy illustrated in Figure S2 and recorded as a percentage of total cell population.

Reverse transcription-polymerase chain reaction analysis

Total RNA was extracted from left lung using TRIZOL ® (Thermo Fisher Scientific, Inc., Waltham, MA) as per manufacturer's instructions. Taqman ® primers used in the PCR reactions including Ccl2, Il6, Tgfb, and Arginase 1 (Arg1) were obtained from Invitrogen. Nuclear pore protein 133 served as an internal control.

Annexin V/PI apoptosis assay, TUNEL staining

Annexin V staining kit (Sigma-Aldrich, MO, US) was used to assess apoptosis in the whole lung. Single cell suspension was obtained from left lung as described above. Cells were then floated in 1x binding buffer and stained with FITC-conjugated Annexin V and PI antibody for 10 minutes and immediately assessed by flow cytometry.

Apoptosis was assessed in paraffin-embedded lung tissue using TACS® TdT *in situ* - Fluorescein TUNEL assay (R&D systems, MN, US) per manufacturer protocol. Briefly, deparaffinized lung

sections were permeabilized using Cytonin for 1 hour and labelled with a combination of Manganese cation, TdT dNTP Mix, and TdT enzyme followed by incubation with Strep-Fluor solution for 20 minutes. Fluorescent imaging and quantification were performed as described above.

Adoptive transfer of MEx treated bone marrow derived monocytes

BMDMy were isolated from 6-8 week-old FVB by flushing the femur and tibia and culturing cells for 3 days in Dulbecco's Modified Eagle Medium (DMEM) supplemented with 10% FBS, containing 30% v/v L929-conditioned medium (as a source of macrophage colony-stimulating factor; M-CSF). Each well was treated with MEx generated from $1x10^6$ MSCs or media only on days 1 and 2. Cells were harvested on day 3 and after two washes with PBS, stained with Dil as per the manufacturer's protocol (Life technologies). BMDMo were then administered via tail vein injection at a one-to-one ratio (BMDMo isolated from one mouse were injected into the experiment mouse, approximately 3×10^6 cells) on day 0 and day 3 after endotracheal instillation of bleomycin.

Adoptive transfer of MEx treated murine derived alveolar macrophages

Six to eight-weeks FVB mice were euthanized by i.p. pentobarbital injection**.** The anterior wall of the trachea was cannulated with a 21-gauge needle and secured using a string. Bronchoalveolar lavage fluid (BAL) was collected with 5 flushes of 0.6 ml of sterile HBSS (supplemented with 0.5 mM EDTA and 1mM HEPES) using a 1 ml syringe. BALF was centrifuged at 400 x *g* for 5 minutes and the supernatant was aspirated. Murine alveolar MΦ were resuspended in fresh RPMI media supplemented with 1% penicillin/streptomycin and 10% FBS and were seeded in a 35 mm plate at a seeding density of $2x10^5$ per plate. Each plate was treated overnight with MEx generated from $2x10^5$ cells. The cells were harvested after 24 hours, washed twice with PBS, stained with Dil and re-suspended in 50 µl of PBS. Alveolar MΦ were administered endotracheally at a one-

to-one ratio (alveolar MΦ isolated from one mouse were administered to the experiment mouse, approximately 6 x 10^5) on day 0 and 3 following instillation of bleomycin.

Liquid chromatography tandem-mass spectrometry (LC-MS/MS)

BMDMo were isolated from WT mice as previously described and treated with MEx (generated from 1x10^6 MSCs) or FEx (exosomes generated from 1x10^6 Fibroblasts) on Day 1 and Day 2. Cells were harvested on day 3 and protein were extracted using the administration of 0.1% SDS buffer.

For LC-MS/MS, a previously published procedure was used (48). Briefly, peptides were desalted using StageTips, dried in a vacuum concentrator and separated by reverse phase chromatography using a Dionex ultimate 3000 RSLC nano UPLC system connected in-line with an Orbitrap Elite (Thermo Fisher Scientific). A database search was performed using Mascot 2.5 (Matrix Science) and SEQUEST in Proteome Discoverer v.1.4. against a murine Uniprot protein database. Data were further processed and inspected in ScaffoldTM 4.8.4 (Proteome Software); quantitative values normalized to total spectra were extracted for downstream analysis.

Bioinformatics analysis

To compare the proteomic profiles of MEx- and FEx-preconditioned bone marrow-derived monocytes (n=4 in each group), lowly abundant peptides were filtered out by keeping features with at least 10 counts in at least 4 samples irrespective of group labels. Following log transformation and quantile normalization, differentially abundant features were identified using a moderated t-statistic as implemented in the limma package from Bioconductor (49). Using an FDR threshold of 0.25, we identified 84 peptides to be differentially abundant between MEx- and FEx-preconditioned bone marrow-derived monocytes, hereafter referred to as the MEx-FEx proteomic signature.

To assess the enrichment of classical and non-classical monocyte genes among the genes encoding for the MEx-FEx proteomic signature, we used a previously published transcriptome data of bone marrow-derived Ly6C^{pos} and Ly6C^{neg} monocytes (29). In brief, raw counts and metadata were obtained from DEE2 database (50). Count data was normalized using the rlog variance stabilization functionality from DESeq2 Bioconductor package (51). Gene annotation was obtained using biomaRt package also from Bioconductor (52), and normalized count data was further summarized at the gene symbol level using the collapseRows functionality from WGCNA R package (53). In the case of more than one ENSEMBL gene id mapping to the same gene symbol, normalized counts from the ENSEMBL id with maximum variance were retained. Finally, self-contained gene set testing was performed using the QuSAGE package from Bioconductor (54). In short, QuSAGE summarizes differential expression of a given gene set by convoluting individual gene t-distributions into a single PDF for the gene set, and tests the null hypothesis that the mean fold change is zero for a comparison of interest. All bioinformatics analysis were performed using the R statistical computing language (55).

Statistics

Data between two groups were compared using 2-tailed Student t-test, and, data between multiple experimental groups were compared using ANOVA with Fisher's LSD *post hoc* analysis in GraphPad Prism (v6.0; GraphPad, CA, US). Flow cytometry data analyses were performed using FlowJo software v10.2 (TreeStar, OR, US). Whole lung mRNA levels were assessed by RT-qPCR relative to endogenous control (Nuclear pore protein 133 (Nup133)), where the ΔCT was used for statistical analysis. Data are presented as mean ± standard deviation (s.d.). Significance was determined with respect to the $p< 0.05$ threshold. For *in vivo* studies, sample size calculations were based on preliminary data (not shown), suggesting that detection of a 20% improvement in lung collagen content with a greater than 90% power at the 5% α-level would require a minimum of 5 animals per experimental group.

Study approval

Animal experiments were approved by the Boston Children's Hospital Animal Care and Use Committee.

Author Contributions

N.M. and G.R.W. participated in study design and execution, data collection, analysis, and manuscript writing; A.F.G. and M.R. participated in study design and execution, analysis and manuscript writing; S.N. performed bioinformatics analyses and contributed to writing the manuscript, S.A.M. and S.K. contributed to study design, supervision of study execution, analysis, manuscript writing, and final article editing and approval.

Acknowledgments

The authors thank Ms. Carolina Medrano and Dr. Roger Ilagan (United Therapeutics Corp, Durham, NC) for useful discussions. We also thank Ms. Xianlan Liu (Boston Children's Hospital, Boston, MA) for expert animal husbandry, Mr. John Daley II and Ms. Susan Lazo (Dana Farber Cancer Institute, Boston, MA) for their flow cytometry expertise and technical assistance, and Dr. Maria Ericsson for supporting electron microscopy experiments (Harvard Medical School, Boston, MA). Mr. Romain Hamelin at the EPFL proteomic facility for helping with sample preparation for mass spectrometry (EPFL, Lausanne, Switzerland).

Funding: This work was supported in part by NIH grants R01HL146128 (S.K.); United Therapeutics Research Grant (S.K. & S.A.M.); American Thoracic Society Foundation Grant (G.R.W.); The Little Giraffe Foundation (G.R.W.); and Charles H. Hood Foundation Major Grants Initiative (SK).

Figures legends

Reference list

1. Gross TJ, Hunninghake GW. Idiopathic pulmonary fibrosis. *N Engl J Med.* 2001;345(7):517-525.
2. Brooks PJ, Samuel LT, Levin JM, et al. Mortality after hip resurfacing versus total hip arthroplasty in young patients: a single surgeon experience. *Ann Transl Med.* 2019;7(4):77.
3. du Bois RM. Idiopathic pulmonary fibrosis: present understanding and future options. *Eur Respir Rev.* 2011;20(121):132-133.
4. Bingle L, Barnes FA, Cross SS, et al. Differential epithelial expression of the putative innate immune molecule SPLUNC1 in cystic fibrosis. *Respir Res.* 2007;8:79.
5. Balestro E, Calabrese F, Turato G, et al. Immune Inflammation and Disease Progression in Idiopathic Pulmonary Fibrosis. *PLoS One.* 2016;11(5):e0154516.
6. Cheresh P, Kim SJ, Tulasiram S, Kamp DW. Oxidative stress and pulmonary fibrosis. *Biochim Biophys Acta.* 2013;1832(7):1028-1040.
7. Kaunisto J, Salomaa E-R, Hodgson U, Kaarteenaho R, Myllärniemi M. Idiopathic pulmonary fibrosis - a systematic review on methodology for the collection of epidemiological data. *BMC Pulmonary Medicine.* 2013;13:1.
8. Aiuti A, Cattaneo F, Galimberti S, et al. Gene therapy for immunodeficiency due to adenosine deaminase deficiency. *The New England journal of medicine.* 2009;360:447-458.
9. Harari S, Caminati A, Madotto F, Conti S, Cesana G. Epidemiology, survival, incidence and prevalence of idiopathic pulmonary fibrosis in the USA and Canada. *Eur Respir J.* 2017;49(1).
10. Toonkel RL, Hare JM, Matthay MA, Glassberg MK. Mesenchymal stem cells and idiopathic pulmonary fibrosis potential for clinical testing. *American Journal of Respiratory and Critical Care Medicine.* 2013;188:133-140.

11. Ortiz LA, Gambelli F, McBride C, et al. Mesenchymal stem cell engraftment in lung is enhanced in response to bleomycin exposure and ameliorates its fibrotic effects. *Proceedings of the National Academy of Sciences of the United States of America.* 2003;100:8407-8411.

12. Ghadiri M, Young PM, Traini D. Cell-based therapies for the treatment of idiopathic pulmonary fibrosis (IPF) disease. *Expert Opinion on Biological Therapy.* 2016;16:375-387.

13. Ortiz LA, Dutreil M, Fattman C, et al. Interleukin 1 receptor antagonist mediates the antiinflammatory and antifibrotic effect of mesenchymal stem cells during lung injury. *Proc Natl Acad Sci U S A.* 2007;104(26):11002-11007.

14. Srour N, Thebaud B. Mesenchymal Stromal Cells in Animal Bleomycin Pulmonary Fibrosis Models: A Systematic Review. *Stem Cells Transl Med.* 2015;4(12):1500-1510.

15. Lee C, Mitsialis SA, Aslam M, et al. Exosomes mediate the cytoprotective action of mesenchymal stromal cells on hypoxia-induced pulmonary hypertension. *Circulation.* 2012;126(22):2601-2611.

16. Heldring N, Mäger I, Wood M, Le Blanc K, El Andaloussi S. Therapeutic potential of multipotent mesenchymal stromal cells and their extracellular vesicles. *Human gene therapy.* 2015;26:506-517.

17. Sdrimas K, Kourembanas S. MSC Microvesicles for the Treatment of Lung Disease: A New Paradigm for Cell-Free Therapy. *Antioxidants & redox signaling.* 2014;21:1905-1915.

18. Willis GR, Kourembanas S, Mitsialis SA. Therapeutic Applications of Extracellular Vesicles: Perspectives from Newborn Medicine. *Methods Mol Biol.* 2017;1660:409-432.

19. Willis GR, Fernandez-Gonzalez A, Anastas J, et al. Mesenchymal Stromal Cell Exosomes Ameliorate Experimental Bronchopulmonary Dysplasia and Restore Lung

Function through Macrophage Immunomodulation. *Am J Respir Crit Care Med.* 2018;197(1):104-116.

20. Cruz FF, Borg ZD, Goodwin M, et al. Systemic Administration of Human Bone Marrow-Derived Mesenchymal Stromal Cell Extracellular Vesicles Ameliorates Aspergillus Hyphal Extract-Induced Allergic Airway Inflammation in Immunocompetent Mice. *Stem cells translational medicine.* 2015;4:1302-1316.
21. Moeller A, Ask K, Warburton D, Gauldie J, Kolb M. The bleomycin animal model: a useful tool to investigate treatment options for idiopathic pulmonary fibrosis? *Int J Biochem Cell Biol.* 2008;40(3):362-382.
22. Barbas-Filho JV, Ferreira MA, Sesso A, Kairalla RA, Carvalho CR, Capelozzi VL. Evidence of type II pneumocyte apoptosis in the pathogenesis of idiopathic pulmonary fibrosis (IFP)/usual interstitial pneumonia (UIP). *J Clin Pathol.* 2001;54(2):132-138.
23. Hagimoto N, Kuwano K, Nomoto Y, Kunitake R, Hara N. Apoptosis and expression of Fas/Fas ligand mRNA in bleomycin-induced pulmonary fibrosis in mice. *Am J Respir Cell Mol Biol.* 1997;16(1):91-101.
24. Gibbons MA, MacKinnon AC, Ramachandran P, et al. Ly6Chi monocytes direct alternatively activated profibrotic macrophage regulation of lung fibrosis. *American Journal of Respiratory and Critical Care Medicine.* 2011;184:569-581.
25. McCubbrey AL, Barthel L, Mohning MP, et al. Deletion of c-FLIP from CD11b(hi) Macrophages Prevents Development of Bleomycin-induced Lung Fibrosis. *Am J Respir Cell Mol Biol.* 2018;58(1):66-78.
26. Misharin AV, Morales-Nebreda L, Reyfman PA, et al. Monocyte-derived alveolar macrophages drive lung fibrosis and persist in the lung over the life span. *The Journal of experimental medicine.* 2017;214:2387-2404.
27. Satoh T, Nakagawa K, Sugihara F, et al. Identification of an atypical monocyte and committed progenitor involved in fibrosis. *Nature.* 2017;541(7635):96-101.

28. Francke A, Herold J, Weinert S, Strasser RH, Braun-Dullaeus RC. Generation of mature murine monocytes from heterogeneous bone marrow and description of their properties.*J Histochem Cytochem*. 2011;59(9):813-25.

29. Mildner A, Schonheit J, Giladi A, et al. Genomic Characterization of Murine Monocytes Reveals C/EBPbeta Transcription Factor Dependence of Ly6C(-) Cells. *Immunity.* 2017;46(5):849-862 e847.

30. Morrison TJ, Jackson MV, Cunningham EK, et al. Mesenchymal Stromal Cells Modulate Macrophages in Clinically Relevant Lung Injury Models by Extracellular Vesicle Mitochondrial Transfer. *Am J Respir Crit Care Med.* 2017;196(10):1275-1286.

31. Hansmann G, Fernandez-Gonzalez A, Aslam M, et al. Mesenchymal stem cell-mediated reversal of bronchopulmonary dysplasia and associated pulmonary hypertension. *Pulm Circ.* 2012;2(2):170-181.

32. Bellon T, Martinez V, Lucendo B, et al. Alternative activation of macrophages in human peritoneum: implications for peritoneal fibrosis. *Nephrol Dial Transplant.* 2011;26(9):2995-3005.

33. Braga TT, Agudelo JSH, Camara NOS. Macrophages during the fibrotic process: M2 as friend and foe. *Frontiers in Immunology.* 2015;6:1-8.

34. Kolahian S, Fernandez IE, Eickelberg O, Hartl D. Immune Mechanisms in Pulmonary Fibrosis. 2016;55:309-322.

35. Mora AL, Torres-Gonzalez E, Rojas M, et al. Activation of alveolar macrophages via the alternative pathway in herpesvirus-induced lung fibrosis. *Am J Respir Cell Mol Biol.* 2006;35(4):466-473.

36. Lin SL, Castano AP, Nowlin BT, Lupher ML, Jr., Duffield JS. Bone marrow Ly6Chigh monocytes are selectively recruited to injured kidney and differentiate into functionally distinct populations. *J Immunol.* 2009;183(10):6733-6743.

37. Desai B, Mattson J, Paintal H, et al. Differential expression of monocyte/macrophage-selective markers in human idiopathic pulmonary fibrosis. *Exp Lung Res.* 2011;37(4):227-238.

38. Greiffo FR FI, Frankenberger M, Ortega-Gomez A, Behr J, Soehnlein O, Eickelberg O. Monocyte immunophenotyping reflects abberant activation patterns in interstitial lung disease patients. *[Abstract] Am J Respir Crit Care Med* 2017;195:A6350.

39. Misharin AV, Morales-Nebreda L, Reyfman PA, et al. Monocyte-derived alveolar macrophages drive lung fibrosis and persist in the lung over the life span. *J Exp Med.* 2017;214(8):2387-2404.

40. van de Laar L, Saelens W, De Prijck S, et al. Yolk Sac Macrophages, Fetal Liver, and Adult Monocytes Can Colonize an Empty Niche and Develop into Functional Tissue-Resident Macrophages. *Immunity.* 2016;44:755-768.

41. Ferguson SW, Wang J, Lee CJ, et al. The microRNA regulatory landscape of MSC-derived exosomes: a systems view. *Sci Rep.* 2018;8(1):1419.

42. Bernard O, Jeny F, Uzunhan Y, et al. Mesenchymal stem cells reduce hypoxia-induced apoptosis in alveolar epithelial cells by modulating HIF and ROS hypoxic signaling. *Am J Physiol Lung Cell Mol Physiol.* 2018;314(3):L360-L371.

43. Dong LH, Jiang YY, Liu YJ, et al. The anti-fibrotic effects of mesenchymal stem cells on irradiated lungs via stimulating endogenous secretion of HGF and PGE2. *Sci Rep.* 2015;5:8713.

44. Wiklander OP, Nordin JZ, O'Loughlin A, et al. Extracellular vesicle in vivo biodistribution is determined by cell source, route of administration and targeting. *J Extracell Vesicles.* 2015;4:26316.

45. Charoenviriyakul C, Takahashi Y, Morishita M, Matsumoto A, Nishikawa M, Takakura Y. Cell type-specific and common characteristics of exosomes derived from mouse cell

lines: Yield, physicochemical properties, and pharmacokinetics. *Eur J Pharm Sci.* 2017;96:316-322.

46. Nichols WW, Murphy DG, Cristofalo VJ, Toji LH, Greene AE, Dwight SA. Characterization of a new human diploid cell strain, IMR-90. *Science.* 1977;196(4285):60-63.

47. Misharin AV, Morales-Nebreda L, Mutlu GM, Budinger GR, Perlman H. Flow cytometric analysis of macrophages and dendritic cell subsets in the mouse lung. *Am J Respir Cell Mol Biol.* 2013;49(4):503-510.

48. Keklikoglou I, Cianciaruso C, Guc E, et al. Chemotherapy elicits pro-metastatic extracellular vesicles in breast cancer models. *Nat Cell Biol.* 2019;21(2):190-202.

49. Ritchie ME, Phipson B, Wu D, et al. limma powers differential expression analyses for RNA-sequencing and microarray studies. *Nucleic Acids Res.* 2015;43(7):e47.

50. Ziemann M, Kaspi A, El-Osta A. Digital expression explorer 2: a repository of uniformly processed RNA sequencing data. *Gigascience.* 2019;8(4).

51. Love MI, Huber W, Anders S. Moderated estimation of fold change and dispersion for RNA-seq data with DESeq2. *Genome Biol.* 2014;15(12):550.

52. Durinck S, Spellman PT, Birney E, Huber W. Mapping identifiers for the integration of genomic datasets with the R/Bioconductor package biomaRt. *Nat Protoc.* 2009;4(8):1184-1191.

53. Langfelder P, Horvath S. WGCNA: an R package for weighted correlation network analysis. *BMC Bioinformatics.* 2008;9:559.

54. Yaari G, Bolen CR, Thakar J, Kleinstein SH. Quantitative set analysis for gene expression: a method to quantify gene set differential expression including gene-gene correlations. *Nucleic Acids Res.* 2013;41(18):e170.

55. R Core Team. R Foundation for Statistical Computing V, Austria. . R: A language and environment for statistical computing. https://www.R-project.org/. Published 2018. Accessed.

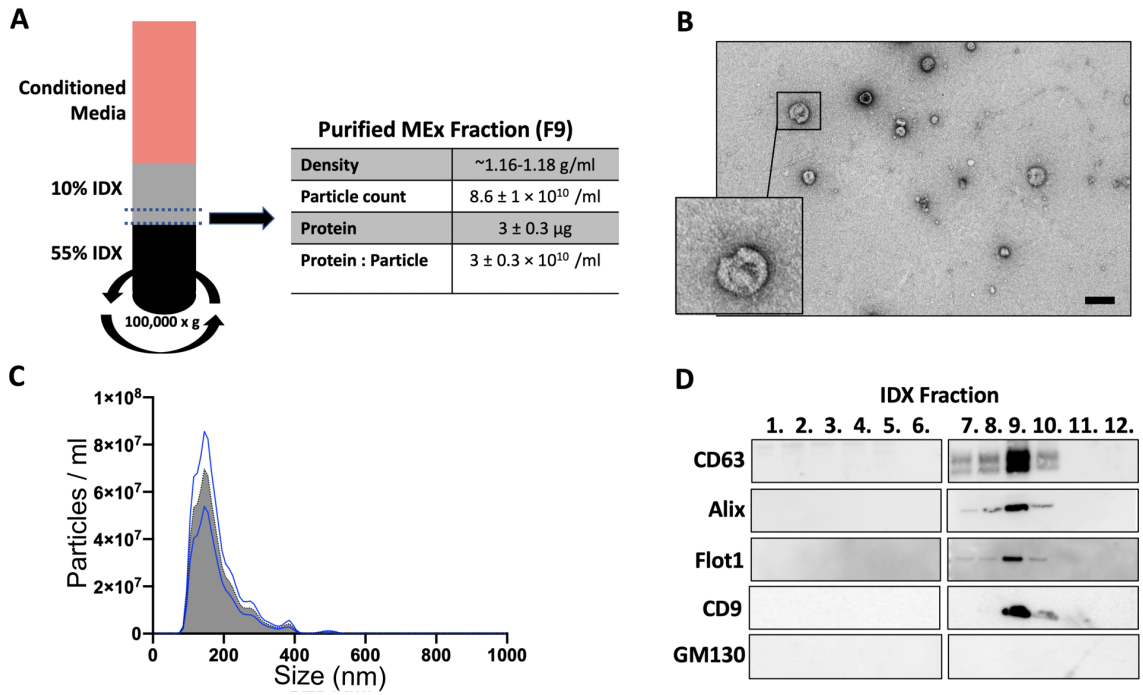

Figure 1: Exosome isolation, purification and characterization. Concentrated conditioned media (CM) was floated on an iodixanol (IDX) cushion gradient and the purify exosome fraction was isolated from fraction 9 (F9), (MEx, Density ~ 1.16-1.18 g/ml). Nanoparticle tracking analysis (NTA) and protein concentration was used to assess exosome concentration and particle:protein ratio in the IDX cushion (12 × 1 ml fractions), respectively (A). Transmission electron microscopy images demonstrating heterogeneous vesicle morphology (scale bar = 500 nm) (B). Size distribution and particle concentration was measured by NTA (C). The IDX cushion gradient fractions were analyzed by Western blot (fraction 1–6 and 7–12, side by side), using antibodies to proteins representing exosome markers. Equivalent volume of each fraction was loaded per lane. Representative images are shown. Flotillin (Flot)-1, Alix and tetraspanins (CD63, CD9) were enriched in fraction 9. GM130 (cytoplasmic marker) was absent in F9.

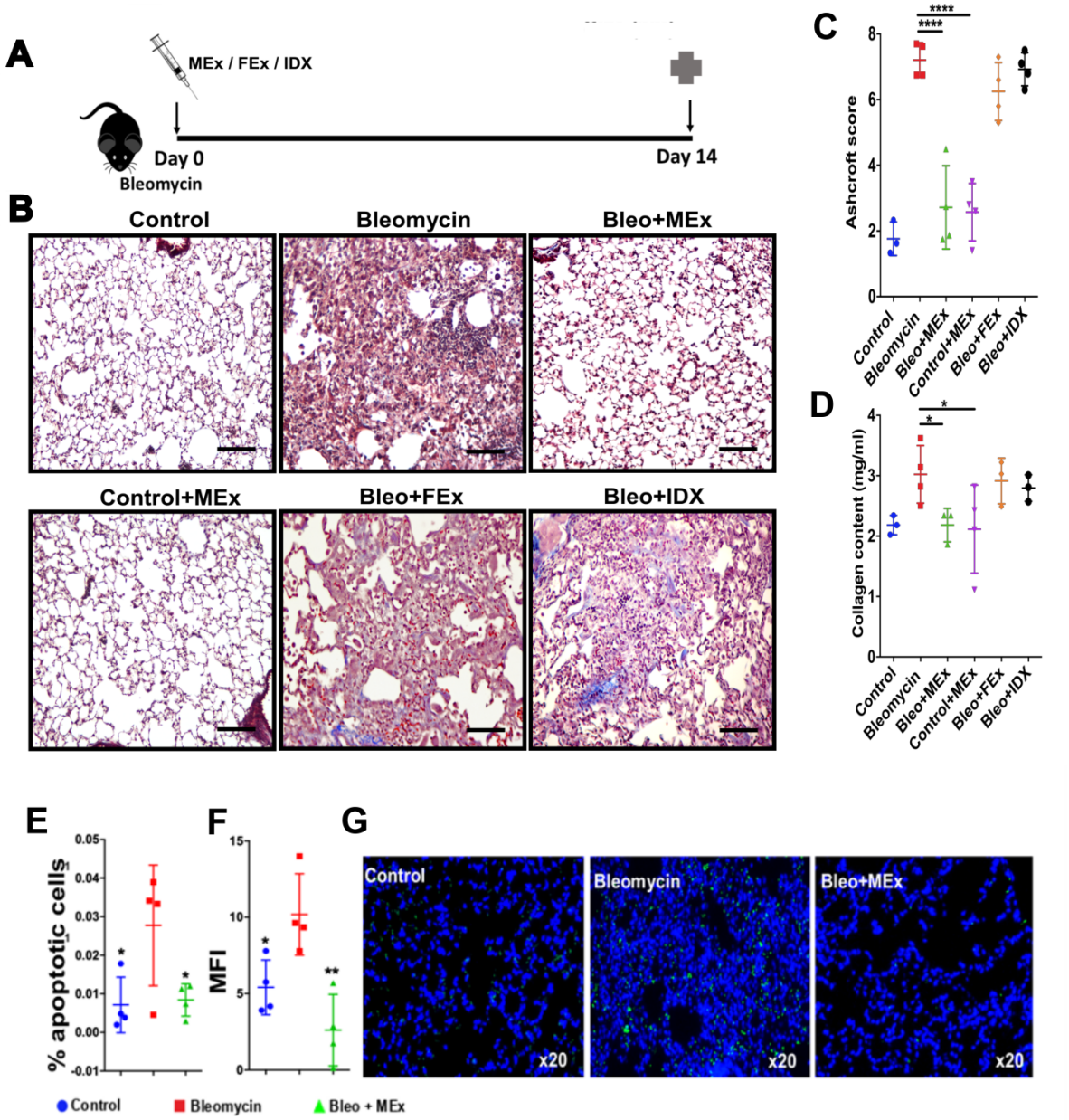

Figure 2: A bolus dose of MEx prevents bleomycin-induced pulmonary fibrosis. Fourteen-week-old mice (C57BL/6 strain) received endotracheal bleomycin (3 U/kg) or 0.9% normal saline on day 0 (control). Concurrently, treated groups received a bolus intravenous (IV) dose of MEx (Bleo+MEx), FEx (Bleo+FEx), or iodixanol (Bleo+IDX). Mice were sacrificed on day 14 (A). Lung sections were stained with Masson's trichrome. Inserts were taken at x100 magnification. Bleomycin, Bleo+FEx, Bleo+IDX showed architectural destruction, alveolar septal thickening

and fibrotic changes. Administration of MEx to bleomycin-challenged mice substantially reduced fibrosis and alveolar distortion (B). Lung fibrosis was measured at day 14 by Ashcroft score (C). Collagen deposition was assessed by Sircol assay and represented as mg/ml of left lung homogenate (D). Data are representative of 3 independent experiments, mean ± s.d. *n* = 3-4 per experimental group, each symbol represents one mouse. *p< 0.05; ****p< 0.0001. 1-way ANOVA followed by Fisher's LSD *post hoc* analysis. Scale bar = 100 μm. **MEx therapy decreases apoptosis.** Annexin V/PI staining in whole lungs shows an increase in apoptosis (Annexin V^+ PI^-) in bleomycin-exposed mice compared to control and bleomycin+MEx mice (E). TUNEL staining in whole lung sections shows increase in apoptosis (green) in the bleomycin-exposed group of mice compared to control and bleomycin+MEx (F, G). Nuclei were stained with Dapi. Images obtained at x 20 magnification. MFI quantified using image J software and normalized for Dapi. Data are representative of 2 independent experiments, mean ± s.d. *n* = 6-8 per group, each symbol represents one mouse, *p< 0.05, ** p< 0.01; vs bleomycin-exposed mice. 1-way ANOVA followed by Fisher's LSD *post hoc* analysis. Abbreviations: MEx, Mesenchymal stromal cell-exosomes; FEx, Human dermal fibroblast-exosomes; IDX, iodixanol; Bleo, bleomycin; PI, Propidium iodide, the cross symbol represents animal harvest.

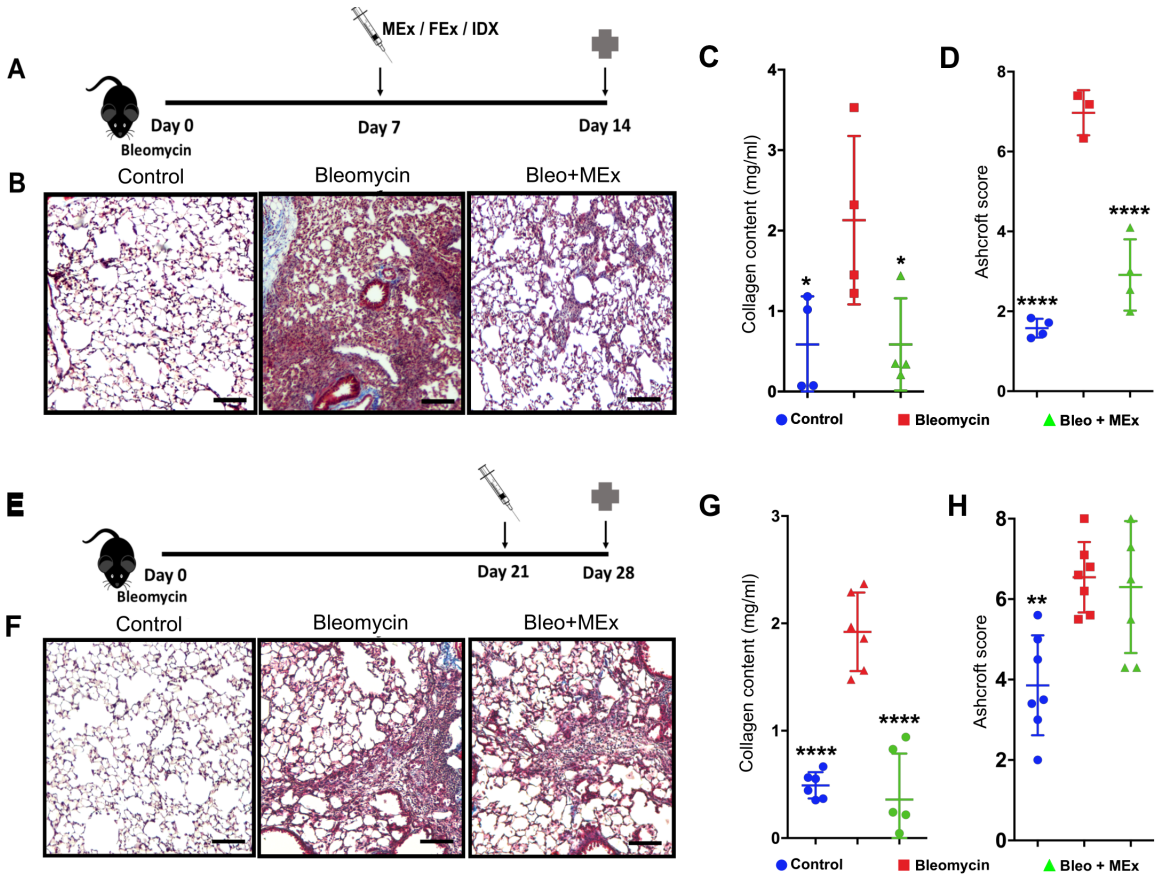

Figure 3: MEx therapy reverts bleomycin-induced pulmonary fibrosis. MEx were administered 7 days or 21 days after the administration of bleomycin and mice were sacrificed on day 14 or 28 (A, E). Lung sections were stained with Masson's trichrome. Inserts were taken at x100 magnification. Representative lung sections from control, Bleomycin and Bleo+MEx mice (B, F). Lung sections were assessed for histology (C, G) and collagen deposition (D,H). Data represent mean ± s.d., Data in panel A-D is representative of 3 independent experiments, *n* = 3-4 per experimental group, Data in panel E-G is representative of 2 independent experiments, *n* = 5-6 per experimental group, each symbol represents one mouse, *p< 0.05; **p<0.01, ****p< 0.0001. 1-way ANOVA followed by Fisher's LSD *post hoc* analysis. Scale bar = 100 µm. Cross symbol represents animal harvest.

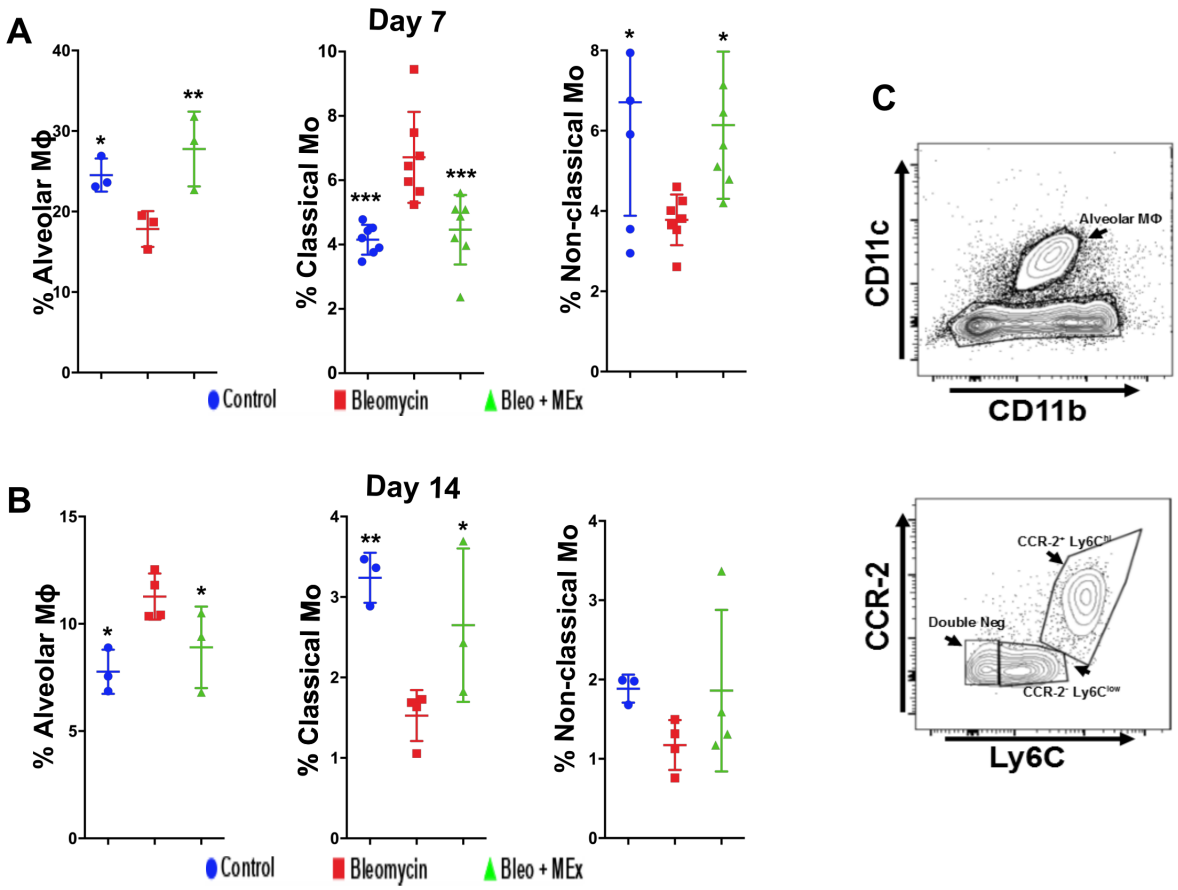

Figure 4: MEx therapy modulates alveolar macrophage and monocyte populations in the lung. Flow cytometry was used to assess whole lung monocyte and alveolar macrophage (alveolar MΦ) at day 7 (A) and day 14 (B). Classical monocytes (Mo) were defined as $CD45^+$ $CD11b^+$ MHC II^- $CD64^-$ $CCR\text{-}2^+$ $Ly6C^{hi}$. Non-classical monocytes were defined as $CD45^+$ $CD11b^+$ MHC II^- $CD64^-$ $CCR\text{-}2^-$ $Ly6C^{low}$. Representative gating strategy of alveolar MΦ, ($CD45^+$ $CD11b^-$ $CD11c^+$ $CD64^+$ cells), Classical Mo and Non-classical Mo (C). The gating strategy was performed according to fluorescence minus one controls (figure S1). Data are representative of 3 independent experiments, Mean ± s.d., n = 4-5 per experimental group, each symbol represents one mouse. *p< 0.05; ** p< 0.01; ***p< 0.001. 1-way ANOVA followed by Fisher's LSD *post hoc* analysis.

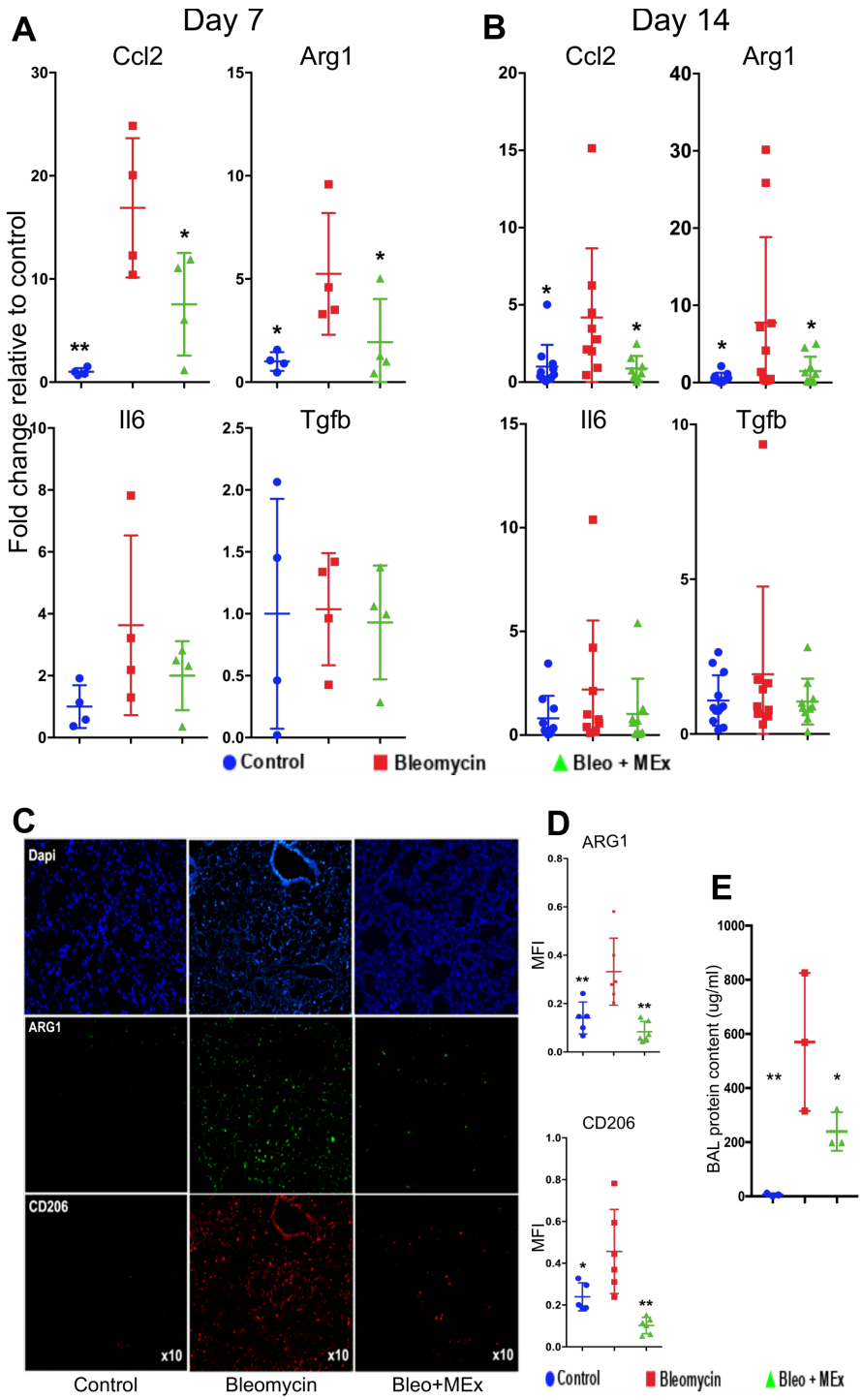

Figure 5: Administration of MEx modulates whole lung inflammation. Whole lung RT-qPCR demonstrated an increase in the mRNA expression levels of *Ccl2* and Arginase1 (*Arg1*) at day 7 and 14 in bleomycin-challenged animals compared to untreated control mice. This was ameliorated by MEx treatment (A, B). Interleukin 6 (*Il6*) expression showed similar trend but

statistical significance was not achieved. Levels of *Tgfb* remained unchanged between the groups. Results are expressed relative to control expression (fold change). Immunofluorescence analysis of lung sections using antibodies against ARG1 (green) and CD206 (red) (C, D). Nuclei staining performed with Dapi (blue). Images obtained at x10 magnification. Mean fluorescence intensity (MFI) normalized for cell number (Dapi stain). Analysis performed by image J software. Mean ± s.d., *n* = 5-8 per group, each symbol represents one mouse, *p<0.05; ** p<0.01. 1-way ANOVA followed by Fisher's LSD *post hoc* analysis. BAL protein content was decreased after MEx treatment (E), Mean ± s.d., *n* = 3-4 per group, each symbol represents one mouse, *p<0.05; ** p<0.01. 1-way ANOVA followed by Fisher's LSD *post hoc* analysis. Abbreviations: BAL, bronchoalveolar lavage; Dapi, 40,6-diamidino-2-phenylindole.

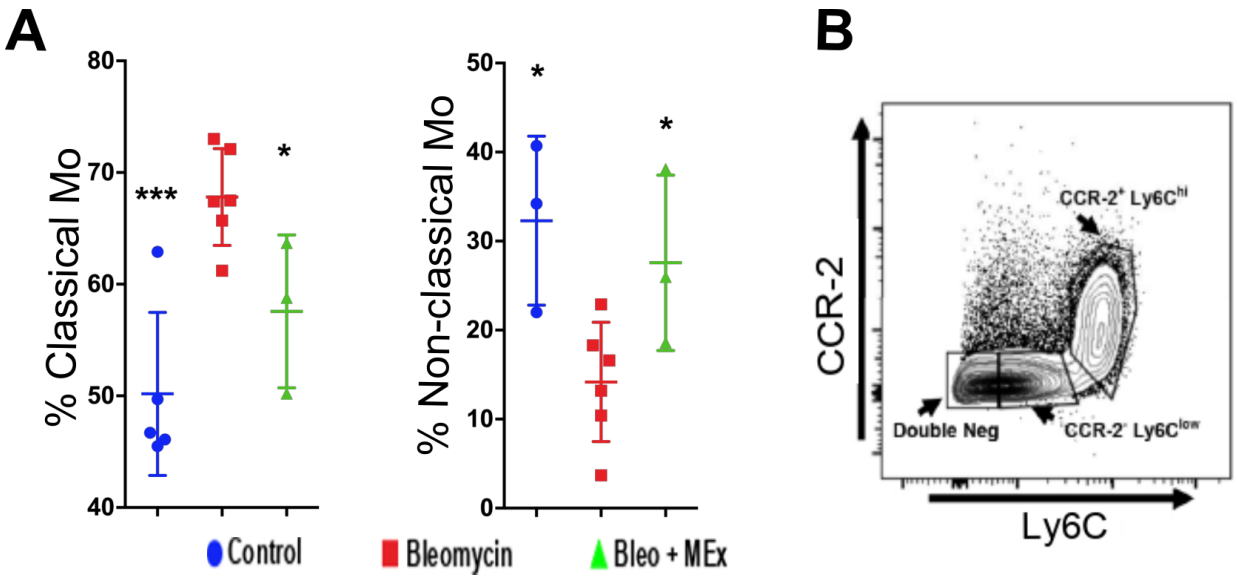

Figure 6: MEx modulate monocyte phenotype in the bone marrow.

To investigate the systemic effects of MEx, we analyzed the myeloid cell profile of the bone marrow at day 7 by flow cytometry. Classical monocytes (Classical Mo) were defined as $CD45^{+}$ $CD11b^{+}$ MHC II^{-} $CD64^{-}$ $CCR\text{-}2^{+}$ $Ly6C^{hi}$. Non-classical monocytes (Non-classical Mo) were defined as $CD45^{+}$ $CD11b^{+}$ MHC II^{-} $CD64^{-}$ $CCR\text{-}2^{-}$ $Ly6C^{low}$ (A). Representative gating strategy (B). Data represents Mean ± s.d., *n* = 5-8 per group, each symbol represents one mouse, *p< 0.05; *** p< 0.001. 1-way ANOVA followed by Fisher's LSD *post hoc* analysis.

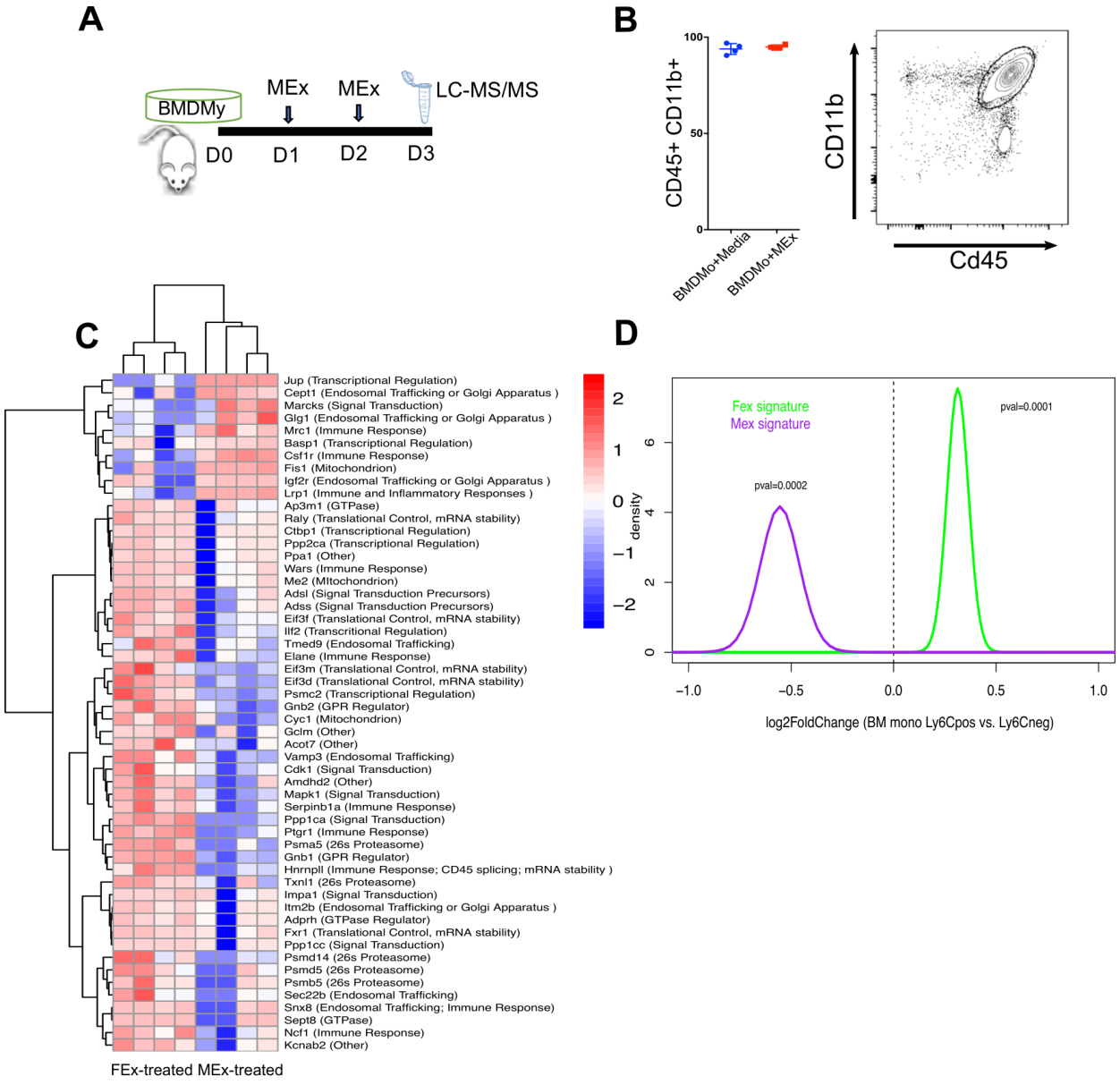

Figure 7: MEx therapy reprograms monocytes to a non-classical (Ly6C^{neg}) phenotype. Bone marrow derived myeloid cells (BMDMy) were isolated from 6-8-wks-old FVB mice, cultured *ex vivo* for 3 days to drive the monocytic lineage and treated with MEx (MEx dose: 1 x 10^6 MSC equivalents) or media alone on day 1 (D1) and day 2 (D2) (A). Flow cytometric analysis of BMDMo after 3 days of culture showed >90% were CD45$^+$ CD11b$^+$ cells. Student's t test (2 tailed) (B). To assess the direct effect of MEx on monocyte phenotype, BMDMo were treated with two doses of MEx or FEx on day 1 and 2, and cells were processed for Liquid Chromatography Tandem Mass

Spectrometry (LC-MS/MS) on day 3 (A). Eighty-four peptides where deemed differentially abundant in MEx-treated BMDMos versus FEx-treated controls at FDR<0.25 (C). Gene set analysis revealed that genes encoding for peptides abundant in MEx-treated BMDMos were on average overexpressed in the $Ly6C^{neg}$ monocytes ($p<0.001$), whereas genes encoding for peptides abundant in the FEx-treated BMDMos were on average overexpressed in the $Ly6C^{pos}$ monocytes ($p<0.001$) (D). Transcriptome data were obtained from GSE95411.

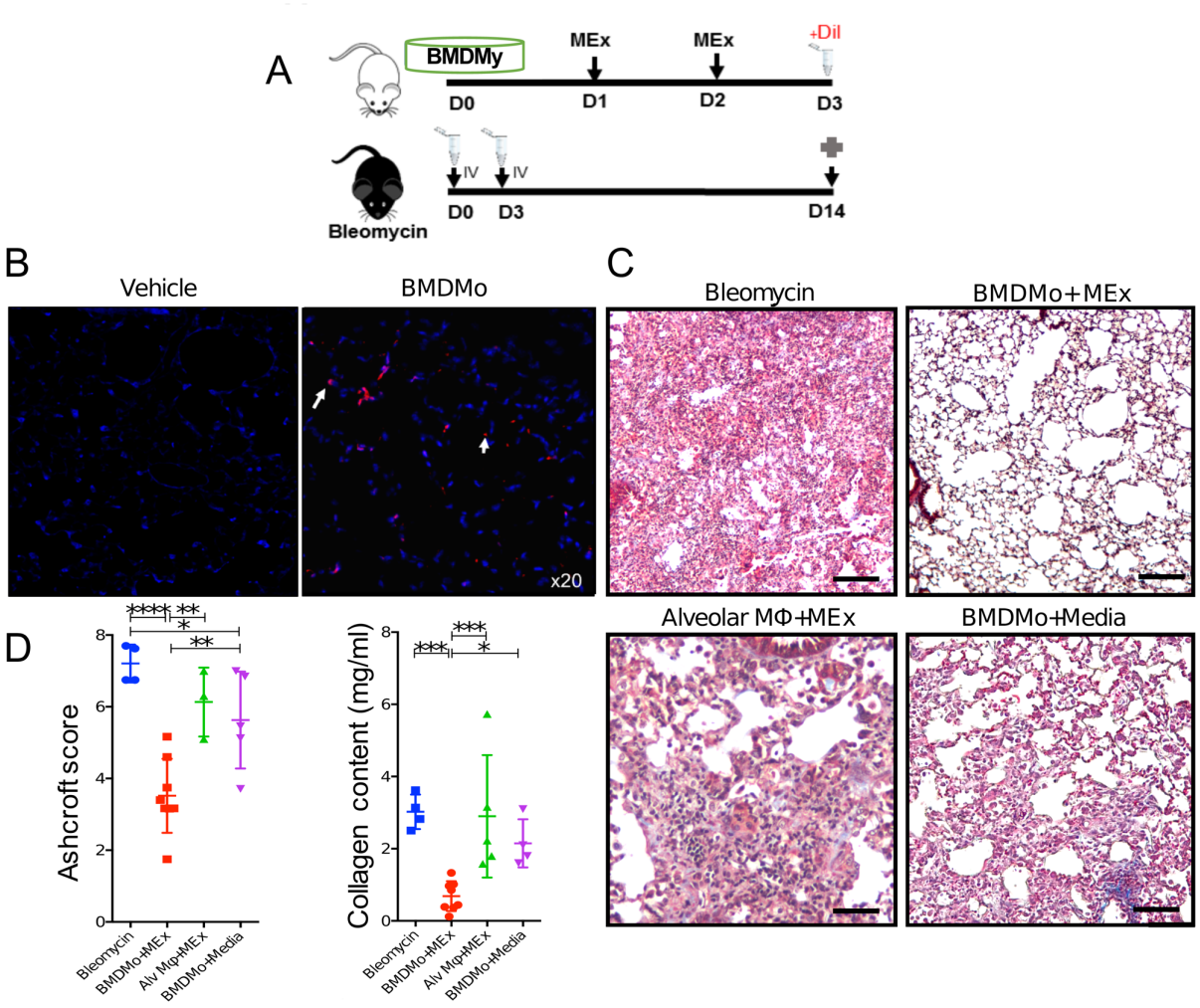

Figure 8: Transplantation of bone-marrow derived-monocytes preconditioned with MEX prevents bleomycin-induced pulmonary fibrosis. We explored the effects of *ex vivo* treated bone marrow derived-monocytes and alveolar macrophages (alveolar MΦ) in the prevention of fibrosis. BMDMo were stained with lipophilic dye (Dil) on day 3 (D3) and intravenously administered at a one-to-one ratio on days 0 and 3 to C57BL/6 mice following endotracheal instillation of bleomycin. Mice were sacrificed at day 14 (A). Dil-labelled BMDMo were detected in the lung 14 days after injection, while no signal was seen in the lung of mice that received cell-free dye (vehicle) (B). Images obtained at x 20 magnification. Pulmonary fibrosis was ameliorated in mice that received monocytes that were preconditioned with MEx, whilst alveolar MΦ had little

effect (C,D,E). Inserts were taken at x 100 magnification. Arrow marks the DiI-labelled monocytes. Data are representative of at least 2 independent experiments, Mean ± s.d., *n* = 4-5 per experimental group, each symbol represents one mouse, Between group comparison: *p< 0.05, ** p< 0.01, ***p< 0.001, ****p< 0.0001. 1-way ANOVA followed by Fisher's LSD *post hoc* analysis. Scale bar = 100 μm. Abbreviations: DiI, 1,1'-Dioctadecyl-3,3,3',3'-Tetramethylindocarbocyanine Perchlorate ('DiI'; DiIC18(3)). Cross symbol represents animal assessment.

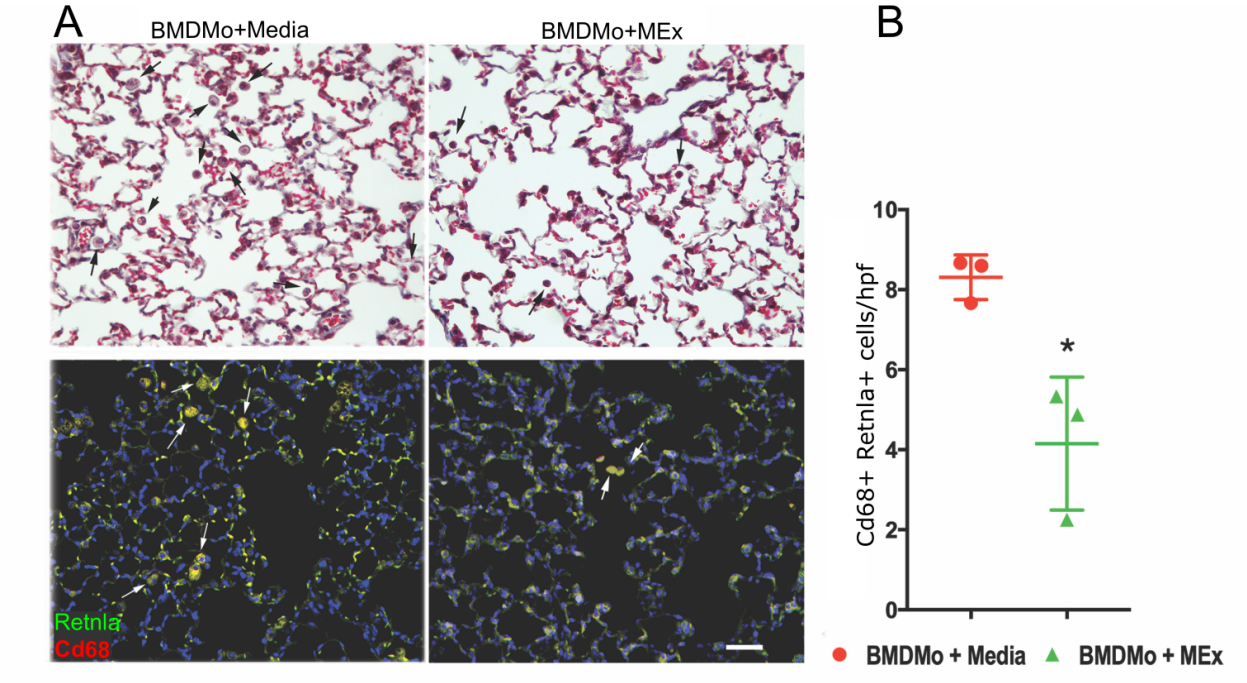

Figure 9: Transplantation of bone-marrow derived-monocytes preconditioned with MEx prevents bleomycin-induced pulmonary inflammation. Pulmonary inflammation was analysed at day 14 after the injection of MEx-preconditioned BMDMo (see details in figure 8) by counting Cd68 and Retnla-expressing macrophages in the pulmonary parenchyma. Mice that received monocytes that were preconditioned with MEx showed reduced macrophage numbers compared to BMDMo+media–treated littermates (A, B). Inserts were taken at x 200 magnification. Arrow marks inflammatory macrophages in alveolar spaces. Data are representative of at least 2 independent experiments, *n* = 3-5 per experimental group, mean ± s.d. Each symbol represents one mouse. Between group comparison: *p< 0.05. Student's t test (2 tailed). Scale bar = 100 µm.